CHEMISTRY OF MATERIALS

pubs.acs.org/cm

Article

Turning Flexibility into Rigidity: Stepwise Locking of Interpenetrating Networks in a MOF Crystal through Click Reaction

Damian Jędrzejowski, Marzena Pander, Wojciech Nitek, Wojciech Bury,* and Dariusz Matoga*

Cite This: *Chem. Mater.* 2021, 33, 7509−7517

Read Online

ACCESS | Metrics & More | Article Recommendations | Supporting Information

ABSTRACT: Post-synthetic modifications of metal−organic frameworks (MOFs) enable synthesis of materials with enhanced performance characteristics or those inaccessible by direct synthetic routes. In this work, for the first time, we utilize inverse-electron demand Diels−Alder (iEDDA) modification to control the structural flexibility and porosity of an open framework material. We selected a series of dienophiles with increasing bulkiness including ethyl vinyl ether (**eve**), cyclohexene (**chx**), norbornene (**nor**), and 5-norbornene-2-methanol (**noh**) to modify a tetrazine-based linker (3,6-dipyridyl-1,2,4,5-tetrazine, **dpt**) incorporated in a unique doubly interpenetrated 3D hybrid MOF−HOF porous material (HOF, hydrogen-bonded organic framework), $\{[Cd_2(coh)_2(dpt)_2]\cdot guests\}_n$ (**JUK-20**). Each subnetwork in **JUK-20** is built of 2D coordination layers stacked by strong complementary C═O···H−N hydrogen bonds between carbohydrazide dibenzoate linkers (**coh**). By using the [4 + 2] click reactions of **JUK-20**, which proceed in a prominent single-crystal-to-single-crystal manner, we obtained a series of **JUK-20-dienophile** MOFs. The modifications lead to a stepwise decrease in structural flexibility of the **JUK-20** platform until the highest rigidity and stability is reached for **JUK-20-noh**. Consequently, the adsorption capacity in the **JUK-20-dienophile** series increases, as revealed collectively by single-crystal X-ray diffraction, physisorption isotherms (N_2, CO_2, and MeOH), and grand canonical Monte Carlo simulations. Our work demonstrates that post-synthetic iEDDA modification is a versatile and efficient tool for systematic functionalization of open framework materials under mild conditions.

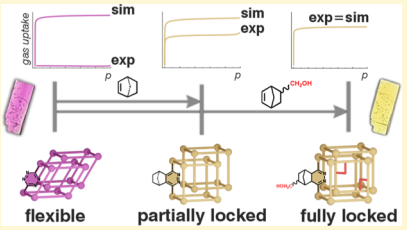

INTRODUCTION

Among various classes of advanced functional materials, metal−organic frameworks (MOFs) stand out by virtue of their unique building units,[1] switchable porosity,[2] and high crystallinity.[3] Large surface areas, tunable pore size, and chemical environment offer a rich landscape for exploring adsorption phenomena and related applications such as gas storage,[4] separation,[5] catalysis,[6] and sensing.[7] From the diversity of metal nodes, organic ligands, and guest molecules emerge a variety of properties whose control can be achieved by taking advantage of the structural flexibility of MOFs. This dynamic behavior of coordination networks can be triggered by external stimuli such as inclusion/removal of guest molecules, pressure, or temperature[8−10] and is governed by two major factors, that is, flexibility of coordination bonds involved in the node-linker interactions and free rotations or bending of structural fragments of the linkers. For interpenetrated systems, additional degrees of freedom must be taken into consideration, arising from separation of individual subnetworks. All these structural features can be collectively manifested as inter- or intraframework movements. Significant changes in flexibility and adsorption properties of a given MOF platform have been observed for various metal ions,[11−13] linkers,[14−16] or their substituents.[17−21] These changes can be realized by rational selection of secondary building units,[11,18,22] post-assembly linker/metal exchange,[23,24] or by covalent post-synthetic modification (CPSM) of linkers.[25−30] Within the last approach, numerous studies have shown classical nucleophilic substitution[31,32] or substitution in a carbonyl group;[33,34] however, these reactions typically require chemically stable structures that are resistant to highly corrosive reagents, for example, acyl chlorides or acid anhydrides. Alternatively, to avoid framework degradation, a number of CPSMs have been carried out under mild conditions using Schiff base condensations,[35,36] reactions between amines and isocyanates,[37,38] or azide−alkyne click reactions.[30,39] On the other hand, these reactions suffer from limitations such as low conversion, products prone to hydrolysis, and necessity to use extra additives or catalysts. Therefore, searching for new post-synthetic irreversible modifications, which can proceed efficiently under mild conditions, is of high importance.

By drawing inspiration from bioorthogonal chemistry[40−43] that occurs in living cells, cycloaddition reactions have been applied as mild CPSM of MOFs.[39] The most common is Huisgen 1,3-dipolar cycloaddition between organic azides and alkynes,[44,45] whereas the variants [2 + 2][46−48] and [4 + 2],

Received: July 15, 2021
Revised: August 24, 2021
Published: September 7, 2021

https://doi.org/10.1021/acs.chemmater.1c02451
Chem. Mater. 2021, 33, 7509−7517

including the Diels–Alder reaction,[49−52] have been rarely employed. The main reason for that is the scarcity of reactive linkers and reversibility of the reactions. The classic variant of the Diels–Alder reaction requires the presence of electron-donor substituents in a diene and electron-acceptor substituents in a dienophile. The major limitations of this approach are high activation energies and the need to use catalysts. An alternative variant of this process called the inverse electron-demand Diels–Alder (iEDDA) reaction reverses the electron requirement between dienes and dienophiles, which broadly expands the library of useful reactants.[42,43,53,54] To date, there are only a handful of literature reports where iEDDA has been reported as CPSM of a coordination polymer.[55−59] The tetrazine-based click reaction in MOFs was initially shown for materials containing an olefin-tagged benzenedicarboxylate linker,[55] and more recently, it was used to obtain a superhydrophobic MOF material[57] or to increase CO_2 adsorption capacity.[59]

Herein, we demonstrate precise control of the number of possible degrees of freedom in a doubly interpenetrated framework by using iEDDA reaction. As a model system, we designed a new MOF platform (**JUK-20**), which contains an immobilized 1,2,4,5-tetrazine entity and enables a series of post-synthetic iEDDA modifications that occur in a unique single-crystal-to-single-crystal (SCSC) manner (Figure 1). Our

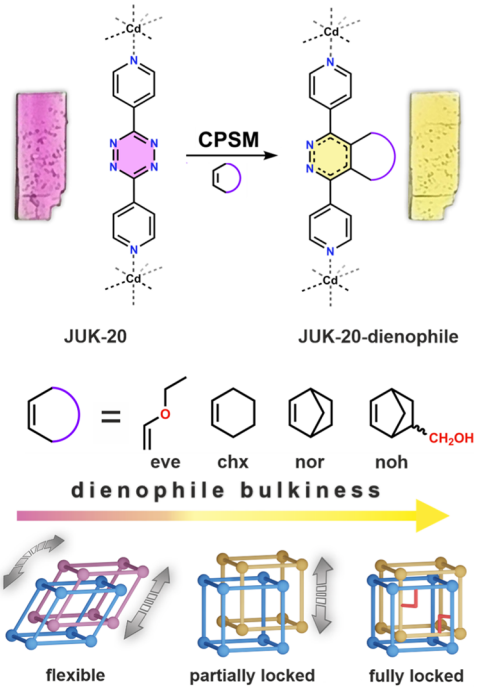

Figure 1. Post-synthetic covalent iEDDA-type modifications (CPSM) of **JUK-20** with dienophiles of increasing bulkiness occurring in an SCSC manner (top). Schematic diagram illustrating control of structural flexibility through CPSM (bottom).

approach allowed for a systematic incorporation of structural fragments with increasing bulkiness and different polarities into the pores of **JUK-20**, which was fully confirmed by SCXRD studies after the iEDDA modifications. The structural flexibility of the parent and daughter materials was thoroughly examined by adsorption of different adsorbates (N_2, CO_2, and MeOH) with varying polarity. Furthermore, the experimental structure–sorption relationship was supported by the grand canonical Monte Carlo (GCMC) simulations. Our work demonstrates that post-synthetic iEDDA modification is an astonishingly versatile and efficient tool for systematic functionalization of open framework materials under mild conditions.

EXPERIMENTAL SECTION

Materials. All reagents and solvents, unless otherwise noted, were purchased from commercial sources and used without further purification. 3,6-Di(pyridin-4-yl)-1,2,4,5-tetrazine (**dpt**) was synthesized by a literature method with a slight modification.[60] Bis(4-formylbenzoic acid) carbohydrazone (**coh**) was synthesized by condensation of carbohydrazide with 4-formylbenzoic acid. (Bicyclo[2.2.1]hept-5-en-2-yl)methanol (**noh**) was synthesized by a literature method.[61] Each derivative of the **dpt** ligand (i.e., **dpt-eve**, **dpt-chx**, **dpt-nor**, **dpt-noh**) was synthesized by iEDDA reaction with a corresponding dienophile (see the Supporting Information for details).

MOF Syntheses. Single crystals of **JUK-20** were obtained by a slow diffusion method. Bulk samples were prepared in closed vials using *N*,*N*-dimethylformamide (DMF)/methanol (MeOH) mixtures at 80 °C. The iEDDA reactions of **JUK-20** with all dienophiles were conducted by using solids suspended in DMF. The reaction conditions were established by monitoring UV–vis and nuclear magnetic resonance (NMR) spectra of the products. Additional control syntheses involving the pre-assembly modified **dpt** linkers (**dpt-eve**, **dpt-chx**, **dpt-nor**, **dpt-noh**) did not lead to **JUK-20-dienophile** products (see the Supporting Information for details).

Physisorption Measurements and GCMC Simulations. The sorption measurements for N_2, CO_2, and methanol were performed at 77, 195, and 293 K, respectively. The virtual porosity of the **JUK-20-x** materials (collective notation for **JUK-20** and **JUK-20-dienophile** series) was analyzed using Zeo++ calculations[62] of the framework models based on the crystal structures (Supporting Information, Table S4). The adsorption isotherms for dinitrogen (77 K), carbon dioxide (195 K), and methanol (293 K) in **JUK-20-x** materials were calculated by GCMC simulations using the RASPA2 software.[63] The models used, simulation, and experimental details are described in the Supporting Information.

RESULTS AND DISCUSSION

Synthesis and Structure of JUK-20. Solvothermal reaction of $Cd(NO_3)_2{\cdot}6H_2O$, **coh**, and **dpt** in DMF/MeOH (9:1 v/v) carried out at 80 °C for 72 h resulted in the formation of $\{[Cd_2(coh)_2(dpt)_2]{\cdot}6DMF{\cdot}5H_2O\}_n$ (**JUK-20**). The phase purity of bulk **JUK-20** was confirmed by comparison of its experimental powder X-ray diffraction (PXRD) pattern with that calculated from single crystal diffraction data (Supporting Information, Figure S1). Single crystals suitable for SC-XRD measurements were obtained by a slow diffusion method (see the Supporting Information for details). **JUK-20** crystallizes in the triclinic space group ($P\bar{1}$) and forms a hybrid MOF–HOF three-dimensional (3D) material (HOF, hydrogen-bonded organic framework). In the structure of **JUK-20**, the **coh** anions act as μ_3-κ^2,κ^2,κ^1 linkers joining bimetallic cadmium clusters, whereas the μ_2-**dpt** ligands act as double pillars and complete the coordination sphere of each metal ion, resulting in the formation of 2D coordination layers of *sql* topology. Importantly, these layers are stacked together by strong complementary C═O···H–N hydrogen bonds between **coh** linkers, forming a 3D hybrid network (Figure 2a). The structure of **JUK-20** consists of two such 3D networks that interpenetrate each other. The relative position of interpenetrating networks is influenced by weak C–H···N interactions and hydrogen bonds with guest solvent molecules (DMF). The as-synthesized **JUK-20** contains open one-

https://doi.org/10.1021/acs.chemmater.1c02451
Chem. Mater. 2021, 33, 7509−7517

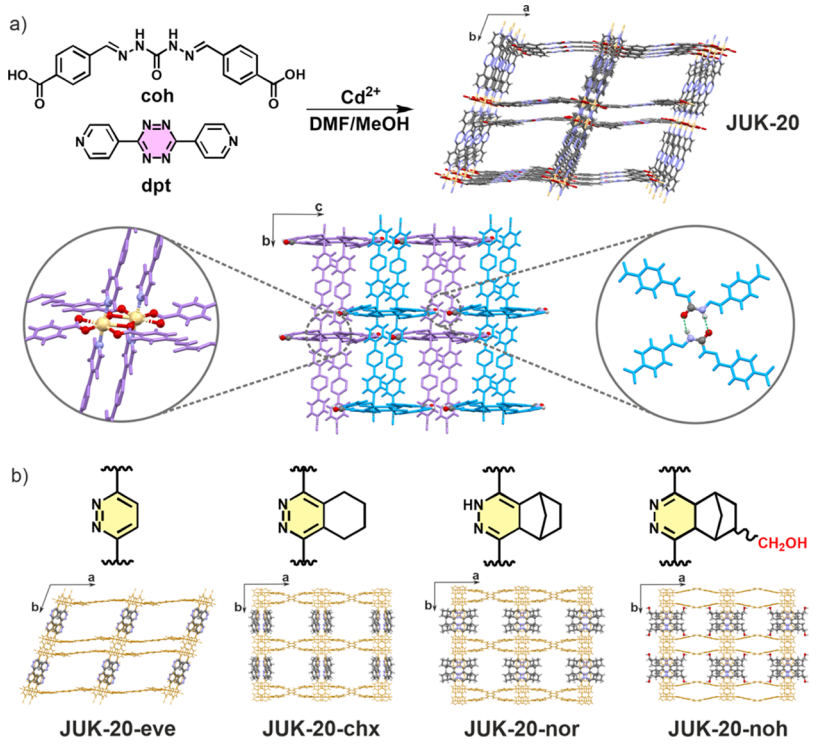

Figure 2. (a) Synthetic scheme leading to microporous **JUK-20** (top); structural features of **JUK-20** (bottom): Cd_2 clusters as nodes (left inset), two interpenetrating hybrid 3D networks (shown as purple and blue), each built of coordination layers stacked by strong hydrogen bonds (right inset). (b) Crystal structures of **JUK-20-dienophile** MOFs with respective tetrazine-derived linkers after iEDDA reactions.

dimensional diamond-shaped channels with large apertures of 10.4 × 17.3 Å propagating along the [001] direction (Figure 2a). The accessible probe-occupiable pore volume of **JUK-20** calculated using the Zeo++ software[62] with a probe radius of 1.86 Å amounts to 45.6%.

Structural features of **JUK-20** are corroborated by vibrational spectroscopy. The infrared (IR) spectrum of **JUK-20** shows characteristic absorption bands corresponding to **coh** and **dpt** ligands (Supporting Information, Figure S1). Apart from symmetric and asymmetric vibrations of carboxylates (1394 and 1535 cm^{-1}, respectively), the presence of 3463, 1668, and 1606 cm^{-1} bands is attributed, respectively, to the amide N−H, C═O, and N═C groups of the **coh** acylhydrazone. A significant blue shift of the amide N−H band as compared to the free **coh** ligand (3222 cm^{-1}) supports the formation of strong hydrogen bonds between the N−H group and the carbonyl oxygen atom. Thermogravimetric analysis of the as-synthesized **JUK-20** demonstrates removal of DMF and H_2O molecules upon heating to ca. 200 °C (weight loss, 27.6%), and the material is thermally stable up to ca. 250 °C (Supporting Information, Figure S1). The desolvation leads to a partial amorphization of **JUK-20**, and its crystallinity is fully recovered upon resolvation (Supporting Information, Figure S2).

Systematic iEDDA Approach to JUK-20-Dienophile MOFs. We hypothesized that the 1,2,4,5-tetrazine as a well-known diene for iEDDA reactions[64] could be a suitable moiety for stepwise introducing of various bulky and anchoring groups into a MOF by proper selection of the dienophiles used for post-synthetic modification. Initially, several iEDDA reactions with various dienophiles were carried out using the **dpt** ligand itself as a reactant (see the Supporting Information for details). Selected dienophiles for the reaction (Figure 2b) included ethyl-vinyl ether (**eve**), cyclohexene (**chx**), norbornene (**nor**), and (norbornenyl)methanol (**noh**), which differ by the presence of electron-donor groups (**eve**, **noh**) and angular stress (**nor**, **noh**). The dienophiles can be arranged in increasing order of reaction rates (**chx** < **eve** < **nor** < **noh**), which strongly correlates with the influence of electron-donor groups and angular stress. The reactions were completed at RT from within several minutes (for **noh**) to several hours (for **chx**). The products were identified and quantified by TLC and NMR spectroscopy. Importantly, direct synthetic approaches toward **JUK-20-dienophile** materials were also explored. **dpt-eve**, **dpt-nor**, and **dpt-noh** were utilized in a series of experiments in different solvents at various concentrations and temperatures. Despite numerous efforts, no pure crystalline phases of **JUK-20-dienophile** MOFs were obtained due to the poor solubility of the modified ligands.

The iEDDA reactions were carried out on single crystals and polycrystalline samples of **JUK-20** immersed in DMF. The reaction progress was monitored visually by observation of dinitrogen gas evolution and a distinct color change from pink to pale yellow (Figure 1 and Supporting Information, Movie S1). The complete conversion was also confirmed by solid-state UV−vis−NIR reflectance spectroscopy; full conversion led to a complete disappearance of the band at 537 nm (Supporting Information, Figure S6). The relative rates for the reactions of **JUK-20** with various dienophiles were the same as for the **dpt** itself; however, due to heterogeneity of the process and diffusion inside the crystals, each reaction time was five to ten times longer than for the ligand.

Structural Studies of the JUK-20-Dienophile Series. The samples after post-synthetic modifications with dienophiles were examined by complementary techniques. The IR spectra after iEDDA reactions show only slight changes in the

https://doi.org/10.1021/acs.chemmater.1c02451
Chem. Mater. 2021, 33, 7509−7517

1390−1410 cm^{-1} range, attributed to the reduced amount of aromatic N−N bonds in the 1,2,4,5-tetrazine moiety, and the appearance of a relatively weak absorption band near 3340 cm^{-1}, from the O−H bond in the **noh** dienophile (Supporting Information, Figure S7). Desolvated samples of the modified **JUK-20** were also subjected to elemental (CHN) and ^1H NMR analyses; the latter were carried out after digestion of the samples in a deuterated sulfuric acid/dimethylsulfoxide-d_6 mixture (Supporting Information, Figure S9). Here, three types of products including 1,2-diazine, 1,4-dihydro-1,2-diazine or 4,5-dihydro-1,2-diazine moieties were identified dependent on the bulkiness of the dienophile and its leaving group (see the Supporting Information for details). The formation of the three products can be rationalized in terms of the commonly accepted cycloaddition mechanism of dienophiles to the 1,2,4,5-tetrazine moiety (Supporting Information, Figures S10−S11). It is worth noting that 4,5-dihydro-1,2-diazine has rarely been reported in the literature as the iEDDA product so far due to its spontaneous oxidation to an aromatic system, and only in the case of a tetrasubstituted dienophile, this product was reported.[65,66]

All post-synthetic iEDDA reactions of **JUK-20** occurred in an SCSC manner and the structures of the products were determined based on SC-XRD (Figure 2b). PXRD patterns for each sample revealed retention of the bulk crystallinity with only slight shifts of the peak positions (Supporting Information, Figure S6). The modification with the **eve** dienophile leads to the replacement of two nitrogen atoms in a tetrazine ring by carbon atoms. A similar modification may be carried out using 2,5-norbornadiene or any other ethylene derivative with a good leaving group. From the network perspective, such a modification is structurally insignificant and causes only slight changes in the unit cell parameters and the accessible pore volumes (V_P) (Table 1). A systematic increase in dienophile bulkiness by incorporating a steric hindrance (**chx**, **nor**, and **noh**) and additionally a hydrogen-bonding group (**noh**) led to the crystal symmetry change from triclinic to monoclinic (Figure 2b) and introduced disorder at the **coh** ligand, which occupied two alternative positions, leading to isomers A (higher pore volume) and B (lower pore volume). Solvent-accessible pore volumes were calculated assuming that the **coh** ligand occupies only one position in each structure (Table 1 and Supporting Information, Table S4). In **JUK-20-chx** and **JUK-20−nor**, the predominant position of the **coh** linker (67 and 75% site occupancies for A isomers, Table 1) is directed outside the main [001] pore, whereas in **JUK-20-noh**, in contrast, this linker occupies mostly the position directed inside the main pore (60% site occupancy for B isomer, Table 1) due to its involvement in hydrogen bonds with the OH group of the **noh** dienophile (Figure 2b). Whereas the shape of the main pore changes significantly from rhomboidal to rectangular upon cycloaddition of bulky dienophiles (**chx**, **nor**, and **noh**), the accessible pore volumes remain practically constant (within 0.03 cm^3/g for **eve** and **chx**) or decrease by 0.10 cm^3/g for **nor** and by 0.15 cm^3/g for **noh,** which is a result of repositioning of the **coh** linker. More importantly, however, the bulky dienophile with a polar substituent (**noh**) provides additional rigidity and stabilization of the framework through strong hydrogen bonding (O−H···O; d(O···O) = 2.82 Å) between adjacent subnetworks. In summary, the least bulky **eve** dienophile does not cause any significant structural changes of **JUK-20**, and the framework flexibility may arise from either intralayer tilting or interlayer displacements. As the bulkiness of dienophiles increases (**chx** and **nor**), the tilt angle becomes fixed at 90° and only 1 degree of freedom remains. Finally, introduction of the bulkiest **noh** dienophile leads to a fully locked rigid structure of **JUK-20-noh**.

Table 1. Selected Geometrical Parameters for JUK-20-x Series Including Structural Disorder

material	γ/deg	site occupancy of **coh** linker	pore volume[a] /$cm^3 \cdot g^{-1}$
JUK-20	70.324	n/a	0.50
JUK-20-eve	69.545	n/a	0.48
JUK-20-chx-A	90	0.67	0.47
JUK-20-chx-B	90	0.33	0.43
JUK-20-nor-A	90	0.75	0.40
JUK-20-nor-B	90	0.25	0.38
JUK-20-noh-A	90	0.40	0.40
JUK-20-noh-B	90	0.60	0.35

[a]Calculated with Zeo++ using a probe radius of 1.86 Å

The susceptibility of undergoing structural changes in **JUK-20-x** materials before and after modification was further investigated by variable-temperature PXRD (VT-PXRD). In Figure 3a, the selected VT-PXRD patterns are shown in a range of 30−300 °C for the **JUK-20-x** series. With increasing temperature, the triclinic **JUK-20** and **JUK-20-eve** materials undergo phase transitions which are confirmed by the appearance of the high-intensity diffraction peaks at higher 2θ angles. In contrast, no visible differences in VT-PXRD patterns can be observed for the rest of **JUK-20-dienophile** materials, hence proving their more rigid nature.

Modulation of Porosity and Flexibility of JUK-20. The structural changes of **JUK-20** upon iEDDA reactions, including the shape of the main [001] channel and interlayer bonding, prompted us to explore the adsorption properties of the **JUK-20-dienophile** series. To estimate the expected virtual porosity of the **JUK-20-x** materials, GCMC calculations were performed based on the structural models of the desolvated frameworks. Structural models for **JUK-20-chx**, **JUK-20-nor**, and **JUK-20-noh** were constructed using the single crystal data including both A and B isomeric frameworks (vide supra, and Supporting Information, Figure S17). The calculated dinitrogen adsorption isotherms are presented in Figure 3b and show that all materials are expected to be porous. Having in hand the simulation data, we performed N_2 adsorption measurements at 77 K on the desolvated MOF powders (Figure 3b). Interestingly, for **JUK-20-x** materials, the comparison of experimental physisorption results with simulations of virtual porosity spreads from a complete disagreement to a perfect match. The largest discrepancies between simulations and measurements were observed for **JUK-20** and **JUK-20-eve**, with the simulated N_2 uptakes of 353 and 340 cm^3/g, respectively. Based on experimental results, **JUK-20** and **JUK-20-eve** are almost non-porous toward dinitrogen, whereas for **JUK-20-chx**, **JUK-20-nor**, and **JUK-20-noh**, we observed significant experimental N_2 uptakes of 230, 266, and 284 cm^3/g, respectively. Surprisingly, the calculated nitrogen adsorption isotherms for **JUK-20-nor** and **JUK-20-noh** are in exceptionally good agreement with the experimental data, that is, the N_2 uptake values of 295 and 278 cm^3/g were obtained, respectively. We ascribe these discrepancies between experiment and simulations to framework flexibility in case of **JUK-20** and **JUK-20-eve**. To further

https://doi.org/10.1021/acs.chemmater.1c02451
Chem. Mater. 2021, 33, 7509−7517

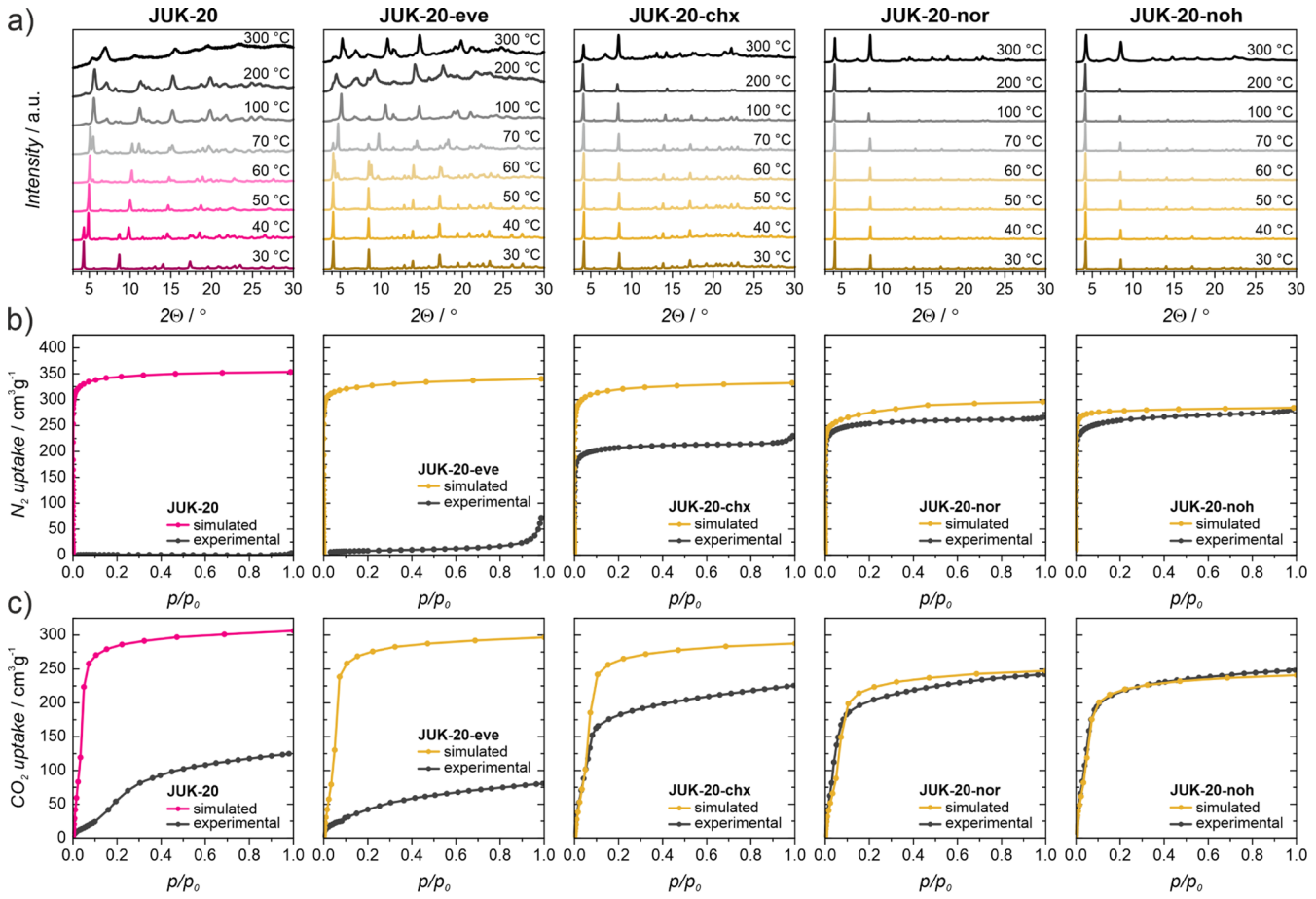

Figure 3. (a) VT-PXRD patterns of the **JUK-20-x** series before and after iEDDA reaction. (b) Nitrogen sorption isotherms (simulated and experimental) measured at 77 K for the **JUK-20-x** series. (c) Carbon dioxide sorption isotherms (simulated and experimental) measured at 195 K for the **JUK-20-x** series. For **JUK-20-chx**, **-nor**, and **-noh**, only the simulated isotherms for the A framework isomers (with higher porosity) are presented.

explore the adsorption properties of the **JUK-20-x** series toward other adsorbates, the CO_2 isotherms were collected at 195 K (Figure 3c) and at 293 K (for **JUK-20** and **JUK-20-noh**, Supporting Information, Figure S15). In contrast to the N_2 physisorption experiments, the porosity toward CO_2 in all **JUK-20-x** materials was observed. Although we noticed significant CO_2 uptake for both **JUK-20** (125 cm^3/g) and **JUK-20-eve** (80 cm^3/g) materials, the obtained values represent only 41 and 27% of the estimated porosities based on GCMC simulations, respectively. These results clearly demonstrate that both structures are porous; however, an adsorbate with a smaller kinetic diameter than that of N_2 is required due to the pore constraints. The CO_2 isotherms of the **JUK-20-chx**, **JUK-20-nor**, and **JUK-20-noh** materials, where more bulky dienophiles were introduced, show much higher CO_2 uptakes of 225, 242, and 248 cm^3/g, respectively. On comparison of the experimental CO_2 sorption isotherms with the isotherms obtained from GCMC simulations (Figure 3c), we noticed particularly good agreement between the simulations and the experiment for **JUK-20-nor** and **JUK-20-noh**, whereas for **JUK-20-chx**, a significant discrepancy is observed (the simulated CO_2 uptake amounts to 287 cm^3/g). We attribute this mismatch to a possible internetwork displacement in the doubly interpenetrated system of **JUK-20-chx** because the **chx** backbone with a moderate bulkiness does not completely prevent possible interframework displacements.

Finally, to further challenge the porosity in the studied **JUK-20-x** systems, we also performed methanol adsorption experiments at 293 K (Supporting Information, Figure S16). The total uptake of MeOH for all the studied materials exceeded 200 cm^3/g at the saturation point, reaching more than 80% of the calculated adsorption capacity for each material. For the most flexible structures, **JUK-20** and **JUK-20-eve**, we observed a significant improvement as compared to N_2 and CO_2 sorption of the methanol-induced structure opening efficiency, which resulted in the maximum CH_3OH uptakes of 234 (simulated—269 cm^3/g) and 218 cm^3/g (simulated—260 cm^3/g), respectively. These results are in good agreement with the simulated MeOH sorption data for those materials in their crystallographic form (Supporting Information, Figure S20). A narrow hysteresis observed in the CO_2 and MeOH isotherms for **JUK-20-nor** and **JUK-20-noh** supports structural rigidity of these frameworks in contrast to the remaining **JUK-20-x** frameworks, where significant hysteresis was observed. The lack of hysteresis in the rigidified MOFs supports the hypothesis that the structural flexibility of the parent MOF has been altered.

Possible Sorption Mechanism in JUK-20-x Materials. Despite the similar total amount of the adsorbed MeOH in all **JUK-20-x** materials, the measured adsorption isotherms

https://doi.org/10.1021/acs.chemmater.1c02451
Chem. Mater. 2021, 33, 7509−7517

(Supporting Information, Figure S16) represent different shapes originating from alternative adsorption mechanisms in these frameworks. The MeOH adsorption isotherm for **JUK-20-chx** exhibits intermediate behavior, which places this framework in the middle of the rigidity scale in the series of **JUK-20-x** materials. Based on the comparison of experimental and simulated adsorption data, we conclude that the most rigid structure is **JUK-20-noh**, which can be treated as a benchmark for mechanistic considerations. Therefore, for this material, we performed a more detailed analysis of snapshots for each adsorption step for CO_2 and MeOH. The snapshots taken at four sorption steps (I–IV, Figure 4) evidently demonstrate a

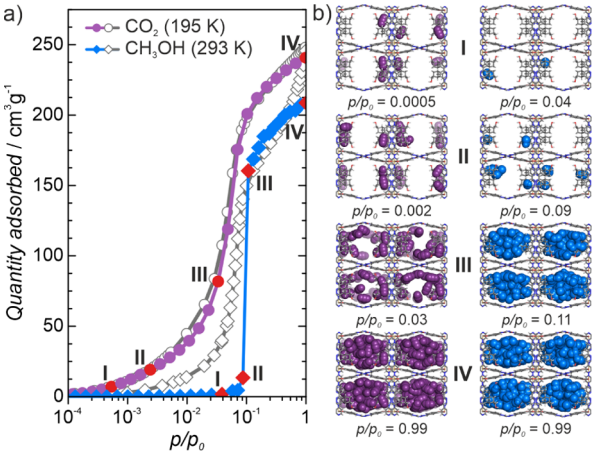

Figure 4. Comparison of simulated and experimental CO_2 (195 K) and MeOH (293 K) adsorption results for **JUK-20-noh**: (a) calculated isotherms (closed symbols) and experimental (open symbols) and (b) adsorption snapshots of CO_2 (left) and MeOH (right) adsorbates taken at selected pressures.

continuous pore filling mechanism for rigid **JUK-20-noh**. The first two snapshots (I and II) clearly show initial adsorption sites for CO_2 molecules, which are located inside baskets formed by the norbornene moieties. In the case of MeOH adsorption, a much steeper isotherm shape was observed for simulated and experimental data (Figure 4).

Moreover, the snapshots taken at four adsorption points for the simulated MeOH isotherm at 293 K demonstrate a slightly different sorption mechanism as compared to CO_2. In this case, at lower pressures of the MeOH vapor (steps I and II, Figure 4), only the norbornene baskets (initial sorption sites) are occupied by MeOH molecules. However, at $p/p_0 = 0.1$, a rapid capillary condensation occurs until complete pore filling with MeOH molecules as shown by a steep increase of the isotherm. Similar behavior was observed for the experimental isotherm, which supports the rigidity of the framework under adsorption conditions. For other materials in the **JUK-20-x** series, various deviations between simulated and experimental isotherms are present as shown in Supporting Information, Figure S20. A similar isotherm trace as for **JUK-20-noh** was obtained for **JUK-20-nor**, which can be explained by similar rigidity of the MOF framework. For more flexible systems, namely, **JUK-20** and **JUK-20-eve**, these discrepancies are more pronounced; the shapes of experimental isotherms suggest continuous opening of the structures without capillary condensation inside large pores.

The importance of increasing the rigidity of MOFs with respect to gas sorption finds support in the paper by Smit and co-workers[67] in which they show that minimizing framework flexibility is an important factor in achieving the globally optimized capacity of an MOF. This work also supports our conclusions that structural flexibility is the cause of low N_2 and CO_2 uptakes for **JUK-20** and **JUK-20-eve**. Apart from the influence on sorption properties, rigidifying MOFs has also been shown in a number of cases to lead to improved light emission properties.[68,69]

CONCLUSIONS

In summary, we have demonstrated that irreversible post-synthetic covalent modification can be utilized for control of flexibility and porosity in an open framework material. By using a unique doubly interpenetrated 3D hybrid MOF-HOF porous material with a tetrazine entity as a model system, we have performed a series of iEDDA reactions with dienophiles of increasing bulkiness and polarity. This systematic approach allowed to introduce various side groups into cavities of the material, which gradually reduced the number of its possible internal motions. The fully locked rigid structure, **JUK-20-noh**, was obtained for the dienophile with a polar anchoring group, capable of strong interaction with pore walls of the adjacent subnetwork. For **JUK-20-noh**, theoretical and experimental adsorption data showed remarkable agreement, whereas for the remaining materials, distinctive discrepancies between theory and experiment were observed and rationalized by their varying degrees of flexibility.

Finally, we envisage the generality of the iEEDA approach and believe that such irreversible click reactions may be used for fine-tuning of structural features and introducing desired functionalities into porous materials under mild conditions. The remaining aromatic nitrogen atoms after CPSM could be used as binding sites for electron-accepting species and the rigidified frameworks could demonstrate the potential for novel gas sorption or sensing properties.

ASSOCIATED CONTENT

Supporting Information

The Supporting Information is available free of charge at https://pubs.acs.org/doi/10.1021/acs.chemmater.1c02451.

Details of synthetic procedures, sample handling, physical measurements, computational studies; additional IR, PXRD, TGA, UV–vis, NMR and adsorption data, crystal structure drawings (PDF).

NMR spectra for the **coh** ligand (ZIP).

CCDC 2065038–2065042 as the supplementary crystallographic data for **JUK-20**, **JUK-20-chx**, **JUK-20-nor**, **JUK-20-noh**, and **JUK-20-eve**. CCDC 2065043–2065045 as the supplementary crystallographic data for **dpt-eve**, **dpt-nor**, and **dpt-noh** (ZIP)

Additional edited **JUK-20-nor** structure. The sets of atomic coordinates and charges of all **JUK-20-x** framework models used for GCMC simulations (ZIP)

iEDDA reaction on a single crystal of **JUK-20** (MP4)

AUTHOR INFORMATION

Corresponding Authors

Wojciech Bury – *Faculty of Chemistry, University of Wrocław, 50-383 Wrocław, Poland;* orcid.org/0000-0002-8207-1384; Email: wojciech.bury@uwr.edu.pl

https://doi.org/10.1021/acs.chemmater.1c02451
Chem. Mater. 2021, 33, 7509–7517

Dariusz Matoga − *Faculty of Chemistry, Jagiellonian University, 30-387 Kraków, Poland;* orcid.org/0000-0002-0064-5541; Email: dariusz.matoga@uj.edu.pl

Authors

Damian Jędrzejowski − *Faculty of Chemistry, Jagiellonian University, 30-387 Kraków, Poland;* orcid.org/0000-0003-1426-2477

Marzena Pander − *Faculty of Chemistry, University of Wrocław, 50-383 Wrocław, Poland;* orcid.org/0000-0003-1681-1353

Wojciech Nitek − *Faculty of Chemistry, Jagiellonian University, 30-387 Kraków, Poland*

Complete contact information is available at: https://pubs.acs.org/10.1021/acs.chemmater.1c02451

Notes

The authors declare no competing financial interest.

■ ACKNOWLEDGMENTS

We gratefully acknowledge the support of the National Science Centre (NCN), Poland; grants no: 2019/35/B/ST5/01067 (D.M., W.N., and D.J.) and 2014/14/E/ST5/00652 (M.P. and W.B). D.J. additionally thanks the Polish Ministry of Science and Higher Education for a doctoral scholarship within the Diamond Grant funding scheme (grant no. 0170/DIA/2019/48). Calculations have been carried out using resources provided by the Wroclaw Centre for Networking and Supercomputing (http://wcss.pl), grant no. 454.

■ ABBREVIATIONS

chx, cyclohexene; CPSM, covalent post-synthetic modification; DMF, *N*,*N*′-dimethylformamide; dpt, 3,6-dipyridyl-1,2,4,5-tetrazine; eve, ethyl-vinyl ether; exp, experimental; GCMC, grand canonical Monte Carlo; H_2coh, bis(4-formylbenzoic acid) carbohydrazone; HOF, hydrogen-bonded organic framework; iEDDA, inverse-electron demand Diels−Alder (reaction); JUK-20, $\{[Cd_2(coh)_2(dpt)_2]\cdot guests\}_n$; JUK-20-dienophile, JUK-20 modified by a dienophile; JUK-20-x, entire JUK-20 platform; MeOH, methanol; MOF, metal−organic framework; NMR, nuclear magnetic resonance; noh, 5-norbornene-2-methanol; nor, norbornene; RT, room temperature; SBU, secondary building unit; sim, simulated; SCSC, single-crystal-to-single-crystal; SC-XRD, single-crystal X-ray diffraction; TLC, thin-layer chromatography; VT-PXRD, variable-temperature powder X-ray diffraction

■ REFERENCES

(1) Furukawa, H.; Cordova, K. E.; O'Keeffe, M.; Yaghi, O. M. The Chemistry and Applications of Metal-Organic Frameworks. *Science* **2013**, *341*, 1230444.

(2) Evans, J. D.; Bon, V.; Senkovska, I.; Lee, H.-C.; Kaskel, S. Four-Dimensional Metal-Organic Frameworks. *Nat. Commun.* **2020**, *11*, 2690.

(3) Feng, L.; Wang, K.-Y.; Day, G. S.; Ryder, M. R.; Zhou, H.-C. Destruction of Metal-Organic Frameworks: Positive and Negative Aspects of Stability and Lability. *Chem. Rev.* **2020**, *120*, 13087−13133.

(4) Mason, J. A.; Veenstra, M.; Long, J. R. Evaluating Metal−Organic Frameworks for Natural Gas Storage. *Chem. Sci.* **2014**, *5*, 32−51.

(5) Li, H.; Wang, K.; Sun, Y.; Lollar, C. T.; Li, J.; Zhou, H.-C. Recent Advances in Gas Storage and Separation Using Metal−Organic Frameworks. *Mater. Today* **2018**, *21*, 108−121.

(6) Bavykina, A.; Kolobov, N.; Khan, I. S.; Bau, J. A.; Ramirez, A.; Gascon, J. Metal−Organic Frameworks in Heterogeneous Catalysis: Recent Progress, New Trends, and Future Perspectives. *Chem. Rev.* **2020**, *120*, 8468−8535.

(7) Li, H.-Y.; Zhao, S.-N.; Zang, S.-Q.; Li, J. Functional Metal−Organic Frameworks as Effective Sensors of Gases and Volatile Compounds. *Chem. Soc. Rev.* **2020**, *49*, 6364−6401.

(8) Vervoorts, P.; Keupp, J.; Schneemann, A.; Hobday, C. L.; Daisenberger, D.; Fischer, R. A.; Schmid, R.; Kieslich, G. Configurational Entropy Driven High-Pressure Behaviour of a Flexible Metal−Organic Framework (MOF). *Angew. Chem., Int. Ed.* **2021**, *60*, 787−793.

(9) Chanut, N.; Ghoufi, A.; Coulet, M.-V.; Bourrelly, S.; Kuchta, B.; Maurin, G.; Llewellyn, P. L. Tailoring the Separation Properties of Flexible Metal-Organic Frameworks Using Mechanical Pressure. *Nat. Commun.* **2020**, *11*, 1216.

(10) Tan, K.; Jensen, S.; Wang, H.; Feng, L.; Wei, K.; Zhou, H. C.; Li, J.; Thonhauser, T. Thermally Activated Adsorption in Metal−Organic Frameworks with a Temperature-Tunable Diffusion Barrier Layer. *Angew. Chem., Int. Ed.* **2020**, *59*, 18468−18472.

(11) Sadakiyo, M.; Yamada, T.; Kato, K.; Takata, M.; Kitagawa, H. A Significant Change in Selective Adsorption Behaviour for Ethanol by Flexibility Control through the Type of Central Metals in a Metal−Organic Framework. *Chem. Sci.* **2016**, *7*, 1349−1356.

(12) Schneemann, A.; Vervoorts, P.; Hante, I.; Tu, M.; Wannapaiboon, S.; Sternemann, C.; Paulus, M.; Wieland, D. C. F.; Henke, S.; Fischer, R. A. Different Breathing Mechanisms in Flexible Pillared-Layered Metal−Organic Frameworks: Impact of the Metal Center. *Chem. Mater.* **2018**, *30*, 1667−1676.

(13) Schneemann, A.; Rudolf, R.; Baxter, S. J.; Vervoorts, P.; Hante, I.; Khaletskaya, K.; Henke, S.; Kieslich, G.; Fischer, R. A. Flexibility Control in Alkyl Ether-Functionalized Pillared-Layered MOFs by a Cu/Zn Mixed Metal Approach. *Dalton Trans.* **2019**, *48*, 6564−6570.

(14) Cao, L.-H.; Liu, X.; Tang, X.-H.; Liu, J.; Xu, X.-Q.; Zang, S.-Q.; Ma, Y.-M. A Fivefold Linker Length Reduction in an Interpenetrated Metal−Organic Framework via Sequential Solvent-Assisted Linker Exchange. *Chem. Commun.* **2019**, *55*, 12671−12674.

(15) Razavi, S. A. A.; Morsali, A. Ultrasonic-Assisted Linker Exchange (USALE): A Novel Post-Synthesis Method for Controlling the Functionality, Porosity, and Morphology of MOFs. *Chem.—Eur. J.* **2019**, *25*, 10876−10885.

(16) Wu, W.; Su, J.; Jia, M.; Li, Z.; Liu, G.; Li, W. Vapor-Phase Linker Exchange of Metal-Organic Frameworks. *Sci. Adv.* **2020**, *6*, No. eaax7270.

(17) Bon, V.; Pallmann, J.; Eisbein, E.; Hoffmann, H. C.; Senkovska, I.; Schwedler, I.; Schneemann, A.; Henke, S.; Wallacher, D.; Fischer, R. A.; Seifert, G.; Brunner, E.; Kaskel, S. Characteristics of Flexibility in Metal-Organic Framework Solid Solutions of Composition [Zn2(BME-Bdc)x(DB-Bdc)2−xdabco]n: In Situ Powder X-Ray Diffraction, in Situ NMR Spectroscopy, and Molecular Dynamics Simulations. *Microporous Mesoporous Mater.* **2015**, *216*, 64−74.

(18) Henke, S.; Schneemann, A.; Wütscher, A.; Fischer, R. A. Directing the Breathing Behavior of Pillared-Layered Metal−Organic Frameworks via a Systematic Library of Functionalized Linkers Bearing Flexible Substituents. *J. Am. Chem. Soc.* **2012**, *134*, 9464−9474.

(19) Chen, T.-H.; Schneemann, A.; Fischer, R. A.; Cohen, S. M. Metal−Organic Frameworks Constructed from Crown Ether-Based 1,4-Benzenedicarboxylic Acid Derivatives. *Dalton Trans.* **2016**, *45*, 3063−3069.

(20) Handke, M.; Weber, H.; Lange, M.; Möllmer, J.; Lincke, J.; Gläser, R.; Staudt, R.; Krautscheid, H. Network Flexibility: Control of Gate Opening in an Isostructural Series of Ag-MOFs by Linker Substitution. *Inorg. Chem.* **2014**, *53*, 7599−7607.

(21) Henke, S.; Schneemann, A.; Kapoor, S.; Winter, R.; Fischer, R. A. Zinc-1,4-Benzenedicarboxylate-Bipyridine Frameworks − Linker Functionalization Impacts Network Topology during Solvothermal Synthesis. *J. Mater. Chem.* **2011**, *22*, 909−918.

(22) Nam, D.-H.; Shekhah, O.; Lee, G.; Mallick, A.; Jiang, H.; Li, F.; Chen, B.; Wicks, J.; Eddaoudi, M.; Sargent, E. H. Intermediate Binding Control Using Metal−Organic Frameworks Enhances Electrochemical CO_2 Reduction. *J. Am. Chem. Soc.* **2020**, *142*, 21513−21521.
(23) Deria, P.; Mondloch, J. E.; Karagiaridi, O.; Bury, W.; Hupp, J. T.; Farha, O. K. Beyond Post-Synthesis Modification: Evolution of Metal−Organic Frameworks via Building Block Replacement. *Chem. Soc. Rev.* **2014**, *43*, 5896−5912.
(24) Karagiaridi, O.; Bury, W.; Mondloch, J. E.; Hupp, J. T.; Farha, O. K. Solvent-Assisted Linker Exchange: An Alternative to the De Novo Synthesis of Unattainable Metal−Organic Frameworks. *Angew. Chem., Int. Ed.* **2014**, *53*, 4530−4540.
(25) Cohen, S. M. Postsynthetic Methods for the Functionalization of Metal−Organic Frameworks. *Chem. Rev.* **2012**, *112*, 970−1000.
(26) Canivet, J.; Aguado, S.; Bergeret, G.; Farrusseng, D. Amino Acid Functionalized Metal−Organic Frameworks by a Soft Coupling−Deprotection Sequence. *Chem. Commun.* **2011**, *47*, 11650−11652.
(27) Kandiah, M.; Usseglio, S.; Svelle, S.; Olsbye, U.; Lillerud, K. P.; Tilset, M. Post-Synthetic Modification of the Metal−Organic Framework Compound UiO-66. *J. Mater. Chem.* **2010**, *20*, 9848−9851.
(28) Fracaroli, A. M.; Siman, P.; Nagib, D. A.; Suzuki, M.; Furukawa, H.; Toste, F. D.; Yaghi, O. M. Seven Post-Synthetic Covalent Reactions in Tandem Leading to Enzyme-like Complexity within Metal−Organic Framework Crystals. *J. Am. Chem. Soc.* **2016**, *138*, 8352−8355.
(29) Kutzscher, C.; Nickerl, G.; Senkovska, I.; Bon, V.; Kaskel, S. Proline Functionalized UiO-67 and UiO-68 Type Metal−Organic Frameworks Showing Reversed Diastereoselectivity in Aldol Addition Reactions. *Chem. Mater.* **2016**, *28*, 2573−2580.
(30) Gadzikwa, T.; Farha, O. K.; Malliakas, C. D.; Kanatzidis, M. G.; Hupp, J. T.; Nguyen, S. T. Selective Bifunctional Modification of a Non-Catenated Metal−Organic Framework Material via "Click" Chemistry. *J. Am. Chem. Soc.* **2009**, *131*, 13613−13615.
(31) Liu, T.; Che, J. X.; Hu, Y. Z.; Dong, X. W.; Liu, X. Y.; Che, C. M. Alkenyl/Thiol-Derived Metal−Organic Frameworks (MOFs) by Means of Postsynthetic Modification for Effective Mercury Adsorption. *Chem.—Eur. J.* **2014**, *20*, 14090−14095.
(32) Britt, D.; Lee, C.; Uribe-Romo, F. J.; Furukawa, H.; Yaghi, O. M. Ring-Opening Reactions within Porous Metal−Organic Frameworks. *Inorg. Chem.* **2010**, *49*, 6387−6389.
(33) Nguyen, J. G.; Cohen, S. M. Moisture-Resistant and Superhydrophobic Metal−Organic Frameworks Obtained via Post-synthetic Modification. *J. Am. Chem. Soc.* **2010**, *132*, 4560−4561.
(34) Wang, Z.; Cohen, S. M. Modulating Metal−Organic Frameworks To Breathe: A Postsynthetic Covalent Modification Approach. *J. Am. Chem. Soc.* **2009**, *131*, 16675−16677.
(35) Dalapati, R.; Biswas, S. Post-Synthetic Modification of a Metal-Organic Framework with Fluorescent-Tag for Dual Naked-Eye Sensing in Aqueous Medium. *Sens. Actuators, B* **2017**, *239*, 759−767.
(36) Huang, A.; Caro, J. Covalent Post-Functionalization of Zeolitic Imidazolate Framework ZIF-90 Membrane for Enhanced Hydrogen Selectivity. *Angew. Chem., Int. Ed.* **2011**, *50*, 4979−4982.
(37) Dugan, E.; Wang, Z.; Okamura, M.; Medina, A.; Cohen, S. M. Covalent Modification of a Metal−Organic Framework with Isocyanates: Probing Substrate Scope and Reactivity. *Chem. Commun.* **2008**, *29*, 3366−3368.
(38) Garibay, S. J.; Wang, Z.; Tanabe, K. K.; Cohen, S. M. Postsynthetic Modification: A Versatile Approach toward Multifunctional Metal-Organic Frameworks. *Inorg. Chem.* **2009**, *48*, 7341−7349.
(39) Li, P.-Z.; Wang, X.-J.; Zhao, Y. Click Chemistry as a Versatile Reaction for Construction and Modification of Metal-Organic Frameworks. *Coord. Chem. Rev.* **2019**, *380*, 484−518.
(40) Sletten, E. M.; Bertozzi, C. R. Bioorthogonal Chemistry: Fishing for Selectivity in a Sea of Functionality. *Angew. Chem., Int. Ed.* **2009**, *48*, 6974−6998.
(41) Jewett, J. C.; Bertozzi, C. R. Cu-Free Click Cycloaddition Reactions in Chemical Biology. *Chem. Soc. Rev.* **2010**, *39*, 1272.
(42) Blackman, M. L.; Royzen, M.; Fox, J. M. Tetrazine Ligation: Fast Bioconjugation Based on Inverse-Electron-Demand Diels-Alder Reactivity. *J. Am. Chem. Soc.* **2008**, *130*, 13518−13519.
(43) Devaraj, N. K.; Weissleder, R.; Hilderbrand, S. A. Tetrazine-Based Cycloadditions: Application to Pretargeted Live Cell Imaging. *Bioconjugate Chem.* **2008**, *19*, 2297−2299.
(44) Goto, Y.; Sato, H.; Shinkai, S.; Sada, K. "Clickable" Metal−Organic Framework. *J. Am. Chem. Soc.* **2008**, *130*, 14354−14355.
(45) Jiang, H.-L.; Feng, D.; Liu, T.-F.; Li, J.-R.; Zhou, H.-C. Pore Surface Engineering with Controlled Loadings of Functional Groups via Click Chemistry in Highly Stable Metal−Organic Frameworks. *J. Am. Chem. Soc.* **2012**, *134*, 14690−14693.
(46) Hazra, A.; Bonakala, S.; Bejagam, K. K.; Balasubramanian, S.; Maji, T. K. Host−Guest [2+2] Cycloaddition Reaction: Postsynthetic Modulation of CO_2 Selectivity and Magnetic Properties in a Bimodal Metal−Organic Framework. *Chem.—Eur. J.* **2016**, *22*, 7792−7799.
(47) Park, I.-H.; Chanthapally, A.; Lee, H.-H.; Quah, H. S.; Lee, S. S.; Vittal, J. J. Solid-State Conversion of a MOF to a Metal-Organo Polymeric Framework (MOPF) via [2+2] Cycloaddition Reaction. *Chem. Commun.* **2014**, *50*, 3665−3667.
(48) Medishetty, R.; Koh, L. L.; Kole, G. K.; Vittal, J. J. Solid-State Structural Transformations from 2D Interdigitated Layers to 3D Interpenetrated Structures. *Angew. Chem., Int. Ed.* **2011**, *50*, 10949−10952.
(49) Nayab, S.; Trouillet, V.; Gliemann, H.; Hurrle, S.; Weidler, P. G.; Rashid Tariq, S.; Goldmann, A. S.; Barner-Kowollik, C.; Yameen, B. Chemically Reprogrammable Metal Organic Frameworks (MOFs) Based on Diels−Alder Chemistry. *Chem. Commun.* **2017**, *53*, 11461−11464.
(50) Nayab, S.; Trouillet, V.; Gliemann, H.; Weidler, P. G.; Azeem, I.; Tariq, S. R.; Goldmann, A. S.; Barner-Kowollik, C.; Yameen, B. Reversible Diels−Alder and Michael Addition Reactions Enable the Facile Postsynthetic Modification of Metal−Organic Frameworks. *Inorg. Chem.* **2021**, *60*, 4397−4409.
(51) Peng, H.; Raya, J.; Richard, F.; Baaziz, W.; Ersen, O.; Ciesielski, A.; Samorì, P. Synthesis of Robust MOFs@COFs Porous Hybrid Materials via an Aza-Diels−Alder Reaction: Towards High-Performance Supercapacitor Materials. *Angew. Chem., Int. Ed.* **2020**, *59*, 19602−19609.
(52) Roy, P.; Schaate, A.; Behrens, P.; Godt, A. Post-Synthetic Modification of Zr-Metal−Organic Frameworks through Cycloaddition Reactions. *Chem.—Eur. J.* **2012**, *18*, 6979−6985.
(53) Pałasz, A. Recent Advances in Inverse-Electron-Demand Hetero-Diels−Alder Reactions of 1-Oxa-1,3-Butadienes. *Top. Curr. Chem.* **2016**, *374*, 1−37.
(54) Prokhorov, A. M.; Kozhevnikov, D. N. Reactions of Triazines and Tetrazines with Dienophiles (Review). *Chem. Heterocycl. Compd.* **2012**, *48*, 1153−1176.
(55) Chen, C.; Allen, C. A.; Cohen, S. M. Tandem Postsynthetic Modification of Metal−Organic Frameworks Using an Inverse-Electron-Demand Diels−Alder Reaction. *Inorg. Chem.* **2011**, *50*, 10534−10536.
(56) Clements, J. E.; Price, J. R.; Neville, S. M.; Kepert, C. J. Perturbation of Spin Crossover Behavior by Covalent Post-Synthetic Modification of a Porous Metal−Organic Framework. *Angew. Chem., Int. Ed.* **2014**, *53*, 10164−10168.
(57) Feng, L.; Lo, S.-H.; Tan, K.; Li, B.-H.; Yuan, S.; Lin, Y.-F.; Lin, C.-H.; Wang, S.-L.; Lu, K.-L.; Zhou, H.-C. An Encapsulation-Rearrangement Strategy to Integrate Superhydrophobicity into Mesoporous Metal-Organic Frameworks. *Matter* **2020**, *2*, 988−999.
(58) Vinu, M.; Sivasankar, K.; Prabu, S.; Han, J.-L.; Lin, C.-H.; Yang, C.-C.; Demel, J. Tetrazine-Based Metal-Organic Frameworks as Scaffolds for Post-Synthetic Modification by the Click Reaction. *Eur. J. Inorg. Chem.* **2020**, *2020*, 461−466.
(59) Zhang, Y.-J.; Nie, H.-X.; Yu, M.-H.; Chang, Z. Post-Synthetic Modification of Tetrazine Functionalized Porous MOF for CO_2

Sorption Performances Modulation. *J. Solid State Chem.* **2021**, *300*, 122257.
(60) Bakkali, H.; Marie, C.; Ly, A.; Thobie-Gautier, C.; Graton, J.; Pipelier, M.; Sengmany, S.; Léonel, E.; Nédélec, J.-Y.; Evain, M.; Dubreuil, D. Functionalized 2,5-Dipyridinylpyrroles by Electrochemical Reduction of 3,6-Dipyridinylpyridazine Precursors. *Eur. J. Org. Chem.* **2008**, *2008*, 2156−2166.
(61) Mammadbayli, E. H.; Hajiyeva, G. E.; Ibrahimli, S. I.; Jafarova, N. A. Mannich Bases from Bicyclo[2.2.1]Hept-5-En-2-Ylmethanol, Secondary Amines and Formaldehyde. *Russ. J. Gen. Chem.* **2018**, *88*, 2204−2208.
(62) Willems, T. F.; Rycroft, C. H.; Kazi, M.; Meza, J. C.; Haranczyk, M. Algorithms and Tools for High-Throughput Geometry-Based Analysis of Crystalline Porous Materials. *Microporous Mesoporous Mater.* **2012**, *149*, 134−141.
(63) Dubbeldam, D.; Calero, S.; Ellis, D. E.; Snurr, R. Q. RASPA: Molecular Simulation Software for Adsorption and Diffusion in Flexible Nanoporous Materials. *Mol. Simul.* **2016**, *42*, 81−101.
(64) Boger, D. L. Diels-Alder Reactions of Heterocyclic Aza Dienes. Scope and Applications. *Chem. Rev.* **1986**, *86*, 781−793.
(65) Hartmann, K.-P.; Heuschmann, M. Steric Effects on the Regioselectivity in Two-Step Diels−Alder Reactions of 1,2,4,5-Tetrazines with 2-Cyclopropylidene-4,5-Dihydro-1,3-Dimethyl-Imidazolidine. *Tetrahedron* **2000**, *56*, 4213−4218.
(66) Mathew, T.; Tonne, J.; Sedelmeier, G.; Grund, C.; Keller, M.; Hunkler, D.; Knothe, L.; Prinzbach, H. [6+6]Photocycloadditions in Face-to-Face Benzo/Pyridazino Substrates − En Route to Azapagodanes. *Eur. J. Org. Chem.* **2007**, *2007*, 2133−2146.
(67) Witman, M.; Ling, S.; Jawahery, S.; Boyd, P. G.; Haranczyk, M.; Slater, B.; Smit, B. The Influence of Intrinsic Framework Flexibility on Adsorption in Nanoporous Materials. *J. Am. Chem. Soc.* **2017**, *139*, 5547−5557.
(68) Bauer, C. A.; Timofeeva, T. V.; Settersten, T. B.; Patterson, B. D.; Liu, V. H.; Simmons, B. A.; Allendorf, M. D. Influence of Connectivity and Porosity on Ligand-Based Luminescence in Zinc Metal−Organic Frameworks. *J. Am. Chem. Soc.* **2007**, *129*, 7136−7144.
(69) Cui, Y.; Yue, Y.; Qian, G.; Chen, B. Luminescent Functional Metal−Organic Frameworks. *Chem. Rev.* **2012**, *112*, 1126−1162.

https://doi.org/10.1021/acs.chemmater.1c02451
Chem. Mater. 2021, 33, 7509−7517